Astron. Astrophys. 343, 367–372 (1999)

ASTRONOMY AND ASTROPHYSICS

A circumnuclear molecular torus in NGC 1365

SEST submillimetre observations of the $J = 3 - 2$ CO line

Aa. Sandqvist

Stockholm Observatory, SE-133 36 Saltsjöbaden, Sweden (aage@astro.su.se)

Received 19 October 1998 / Accepted 3 December 1998

Abstract. The central region of NGC 1365 has been mapped in the $J = 3 - 2$ CO emission line with the 15 m SEST, which has a HPBW of 15″ at the frequency of this transition. The observing grid has a 5″-spacing in the inner and a 10″-spacing in the outer region. A deconvolved map has been produced using the Maximum Entropy Method (MEM). A circumnuclear molecular torus with a radius of about 6.″5 is the dominant feature. Molecular emission is also seen coming from various dust streamers in the bar of the galaxy. Four new molecular species have been detected in NGC 1365, namely HCN, HCO^+, H_2CO and CS. ^{13}CO has also been observed in the nuclear region.

Key words: radio lines: galaxies – galaxies: Seyfert – galaxies: nuclei – galaxies: ISM – galaxies: individual: NGC 1365

1. The central regions of NGC 1365

NGC 1365 is a prominent barred spiral galaxy in the Fornax cluster with a heliocentric velocity of +1632 km s^{-1} (see Lindblad 1999 for an extensive review). The galaxy displays a wide range of phenomena indicating activity – including a Seyfert 1.5 type nucleus with strong, broad and narrow Hα lines and ejection of hot gas from the nucleus (Véron et al. 1980; Jörsäter et al. 1984; Jörsäter & Lindblad 1989). The nucleus is a moderately strong infrared source as seen by IRAS (Lonsdale et al. 1985; Ghosh et al. 1993). The nuclear region contains an extended X-ray source. In addition, there are several discrete X-ray sources within the optical image of the galaxy, one of which is highly variable (Turner et al. 1993; Iyomoto et al. 1997; Komossa & Schulz 1998). At an assumed distance of 18.6 Mpc (Madore et al. 1998), 1″ corresponds to 90 pc.

At Stockholm Observatory, we have been studying the central region of NGC 1365 in great detail also in the radio region using the VLA, the NRAO 12-m millimeter wave telescope and the 15-m SEST (Sandqvist et al. 1982, 1988, 1995; Jörsäter & van Moorsel 1995). Strong CO emission peaks near the inner edges of the bar dust lanes, close to the central regions of starburst activity, and a number of radio sources form a ring-like structure around the edge of a rotating nuclear disk which coincides with the general region of optical hot spots. Our VLA continuum observations show that some of the radio sources are smaller than 0.″1 and we have suggested that they may be radio supernovae. At the core of the galaxy there is a weak, steeply non-thermal radio source from which emanates a 5″-long radio jet, which is also steeply non-thermal (Sandqvist et al. 1995). The jet is aligned along the symmetry axis of a conical shell of hot ionized [O III] gas and both are projected along the minor axis of the galaxy (Hjelm & Lindblad 1996). Kristen et al. (1997) have used the Hubble Space Telescope to study the Seyfert nucleus and nuclear hot spots in NGC 1365 and find these hot spots to be resolved into a number of bright compact condensations. One of these condensations (SSC:10) coincides exactly with a radio source (A). Kristen et al. interpret these condensations as super star clusters (SSC) and the radio source as a radio supernova in one of these clusters.

Molecular gas has previously been mapped in the bar and central region of the Seyfert galaxy NGC 1365 with the SEST using the $J = 1 - 0$ and $2 - 1$ CO lines with resolutions of 44″ and 25″, respectively (Sandqvist et al. 1995). The CO molecular gas is strongly concentrated to the nucleus, where the CO integrated line intensity has a maximum, and the global CO distribution falls off roughly exponentially with the distance from the centre of the galaxy. There is some CO alignmnent with the dust lanes in the bar and some weak emission has been detected in the western spiral arm near the end of the bar at the position of a major H I concentration observed by Jörsäter & van Moorsel (1995). The central CO luminosity corresponds to a molecular hydrogen mass of 5.4×10^9 M$_\odot$ within a projected radius of 2.0 kpc. The global molecular hydrogen gas mass is 17×10^9 M$_\odot$, which is similar to the total amount of neutral atomic hydrogen, 13×10^9 M$_\odot$, found by Jörsäter & van Moorsel (1995) using the VLA. (Here we have rescaled the published values due to the change in adopted distance of NGC 1365 from 20 to 18.6 Mpc). The distribution of the H I is, however, radically different from that of the CO. Whereas the molecular mass is concentrated to the nucleus and bar region, the H I is predominantly located in the spiral arm regions. In particular, the H I distribution shows a hole in the central region which coincidies with the CO emission. This indicates that the gas is predominantly molecular in the centre and the inner bar regions.

We have carried out new observations of the central region of NGC 1365, predominantly in the $J = 3 - 2$ CO line, but

Send offprint requests to: Aage Sandqvist

also in other molecular line transitions in the millimetre wave region (for preliminary reports, see Sandqvist 1996 and Kristen et al. 1998). Since the $J = 3 - 2$ CO line is excited in regions of higher excitation and density than the $J = 2 - 1$ and $1 - 0$ lines, it is a good probe of the molecular gas as it passes through the shocks in the inner bar. The higher resolution offered by the $J = 3 - 2$ line observations also enables a better comparison with the Inner Lindblad Resonances and with predictions of molecular gas kinematic transport inward along the bar to the central star burst region, expected from numerical simulations of gas flow in this galaxy (Lindblad et al. 1996).

2. Millimetre and submillimetre observations with SEST

Observations of NGC 1365 were carried out in August 1995 using the 15-m Swedish ESO-Submillimetre Telescope (SEST) on La Silla in Chile. During the first four nights of the observing run, the atmospheric conditions were excellent, permitting submillimetre observations of the $J = 3 - 2$ CO line. The weather then deteriorated somewhat, forcing a change to the millimetre wavelength region. The telescope properties at the observed frequencies are presented in Table 1.

A dual beam switch mode, with a beam separation of 11′.6, was used placing the source alternatively in the two beams to eliminate asymmetries in the signal paths. Three different SIS receivers were used in conjunction with two low-resolution acousto-optical spectrometers, each with a total bandwidth of about 1 GHz (channel resolution of 1.4 MHz). The average receiver temperatures ($T_{\rm receiver}$) are given in Table 1, as are the channel velocity resolutions after smoothing operations. Only linear baseline subtractions were performed on the profiles. All profile temperatures have been converted to main beam brightness temperatures $(T_{\rm mb})$ by dividing the antenna temperatures $(T_{\rm A}^*)$ by the respective main beam efficiencies $(\eta_{\rm mb})$. The velocities are heliocentric radial velocities.

Four new molecular species have been detected in NGC 1365, namely HCN, HCO^+, H_2CO and CS. These four profiles are presented in Fig. 1 together with that of $J = 1 - 0$ ^{13}CO. All five species are tracers of high density gas. The integrated main beam brightness line intensities, $\int T_{\rm mb} dV$, are HCN: 4.91, HCO^+: 4.25, ^{13}CO: 7.61, H_2CO: 0.93 and CS: 2.21 K km s^{-1}. The $T_{\rm mb}$ rms noise levels of the profiles are of the order of 0.002 K. Submillimetre $J = 3 - 2$ CO line profiles observed towards three positions in the centre of NGC 1365 are also presented in Fig. 1; the equatorial offsets from the optical nucleus for these observations are given in square brackets. The total integrated CO line intensities, $\int T_{\rm mb} dV$, are 276 and 277 K km s^{-1} at the southwest and northeast maxima, respectively; at the centre, this value is 236 K km s^{-1}.

The mapping in the $J = 3 - 2$ CO line was done over an approximately $120'' \times 60''$ region, centered on the optical nucleus $(\alpha(1950.0) = 3^{\rm h}31^{\rm m}41\overset{\rm s}{.}80, \delta(1950.0) = -36°18'26\overset{''}{.}6)$ and covering the bar region. A total number of 133 positions were observed. A grid spacing of 10″ was used for the outer parts of this region. For the inner part (approximately $70'' \times 40''$) a grid spacing of 5″ was used, i.e. a sampling rate of three points per HPBW. Great care was applied to frequent pointing checks. This included using the central profile of NGC 1365 as a pointing check, since an error of a few arcseconds would be immediately noticeable in the relative amplitudes of the two main components in the central profile. Furthermore, observations of the inner part were made only during night time, after midnight and before sunrise, which is the time of maximum atmospheric stability. In addition, observations were only made at elevations between 50° and 80° in order to minimize beam distortion and maximize aperture efficiency. A profile map including all the $J = 3 - 2$ CO observations is presented in Fig. 2.

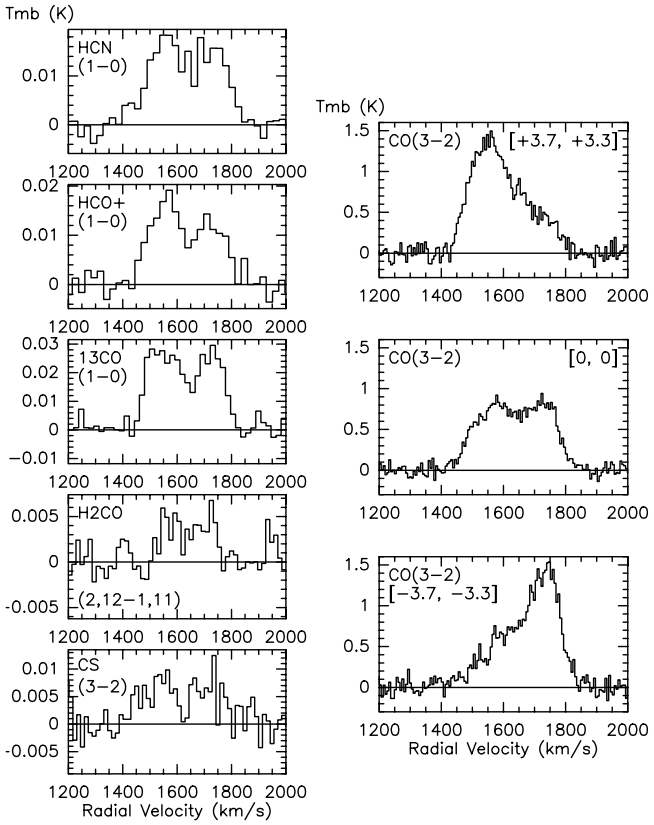

Fig. 1. *Left*: Millimetre molecular line profiles observed towards the central position in NGC 1365. *Right*: Submillimetre $J = 3 - 2$ ^{12}CO molecular line profiles observed towards three positions in the centre of NGC 1365. The equatorial offsets from the optical nucleus (inside square brackets) are given in arcseconds

3. The CO distribution and velocity structure

A map of the total integrated $J = 3 - 2$ CO line intensity $\int T_{\rm mb} dV$-distribution is presented in Fig. 3. The interrelation between the emission regions of the CO molecular line, the dust lanes and the H II hot spot regions in the central region of NGC 1365 has already been presented in a conference proceedings (Sandqvist 1996), where the CO contours were superimposed upon a $B - {\rm Gunn}z$ colour index map. In this paper we make a similar comparison – see Fig. 6 – but use instead a Maximum Entropy Method deconvolved map of the CO emission, which we describe in Sect. 4.

Table 1. SEST parameters and observational results

Frequency (GHz)	Molecule	Transition	HPBW ($''$)	$\eta_{\rm mb}$	$T_{\rm receiver}$ (K)	Channel Resolution (km s^{-1})	$T_{\rm mb}$ (K)	$\int T_{\rm mb} dV$ (K km s^{-1})
88.6	HCN	$(1-0)$	57	0.92	100	22	0.018	4.91
89.2	HCO^+	$(1-0)$	57	0.92	100	22	0.018	4.25
110	^{13}CO	$(1-0)$	48	0.82	110	19	0.027	7.61
141	H_2CO	$(2_{1,2}-1_{1,1})$	36	0.68	130	15	0.005	0.93
147	CS	$(3-2)$	34	0.66	135	14	0.007	2.21
346	^{12}CO	$(3-2)$	15	0.26	425	6	0.80	236

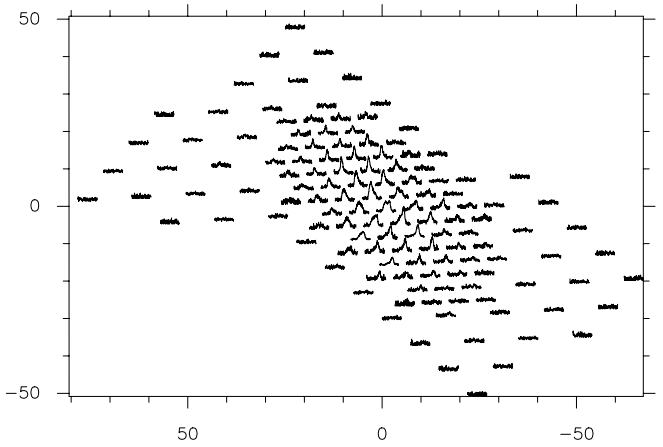

Fig. 2. $J = 3-2$ CO profile map of NGC 1365. The equatorial offsets are in units of arcseconds and are measured from the optical nucleus

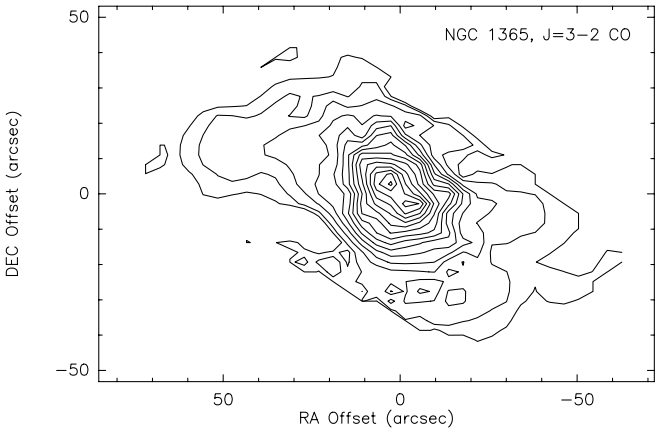

Fig. 3. The $\int T_{\rm mb} dV$-distribution of the $J = 3-2$ CO emission line. The two lowest contour values are 7.7 and 19.2 K km s^{-1}, thereafter the contour interval is 19.2 K km s^{-1}. The equatorial offsets are in units of arcseconds and are measured from the optical nucleus

There is clear correspondence between the extended CO emission, as represented by the outermost contours, and the dust lanes at the preceding edges of the bar. Even the curved dust feature near the western end of the bar has a corresponding distinctly curved CO component, which can be seen in the lowest contour level. Other dust streamers also contain observable CO.

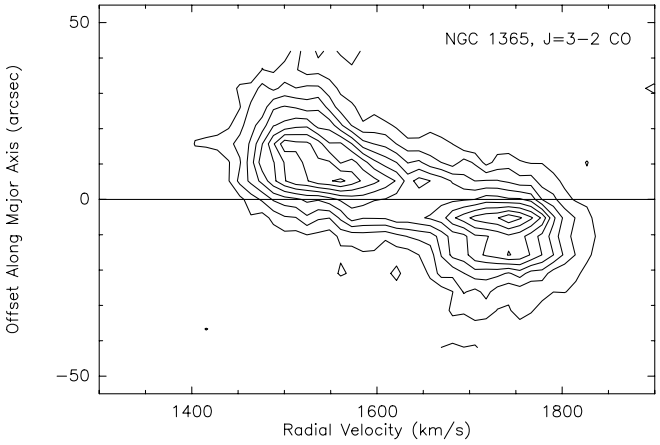

Fig. 4. $J = 3-2$ $T_{\rm mb}$ CO position-velocity map along the major axis of NGC 1365; northeast is up and southwest is down. The lowest contour value and the contour interval are 0.15 K

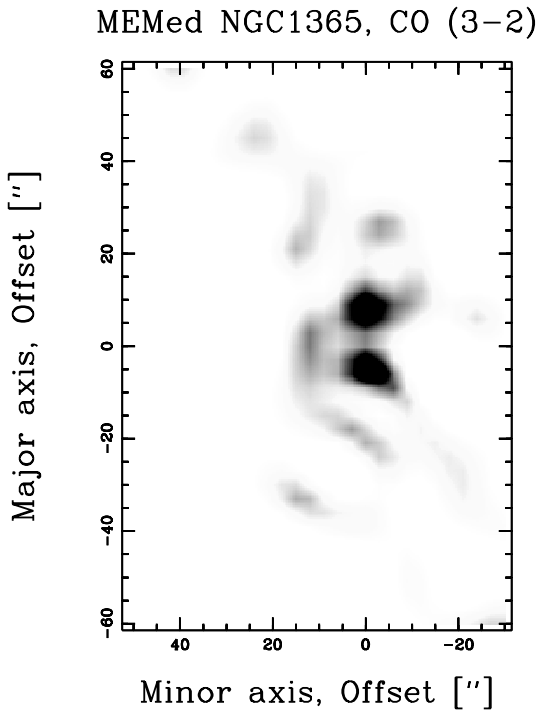

Fig. 5. SEST MEM grey-scale map of NGC 1365 (effective resolution $5''$) in the $J = 3-2$ CO line over an approximately $120'' \times 60''$ region, centered on the optical nucleus and covering the bar; the image has been rotated clockwise by 48°; northeast is up and southwest is down

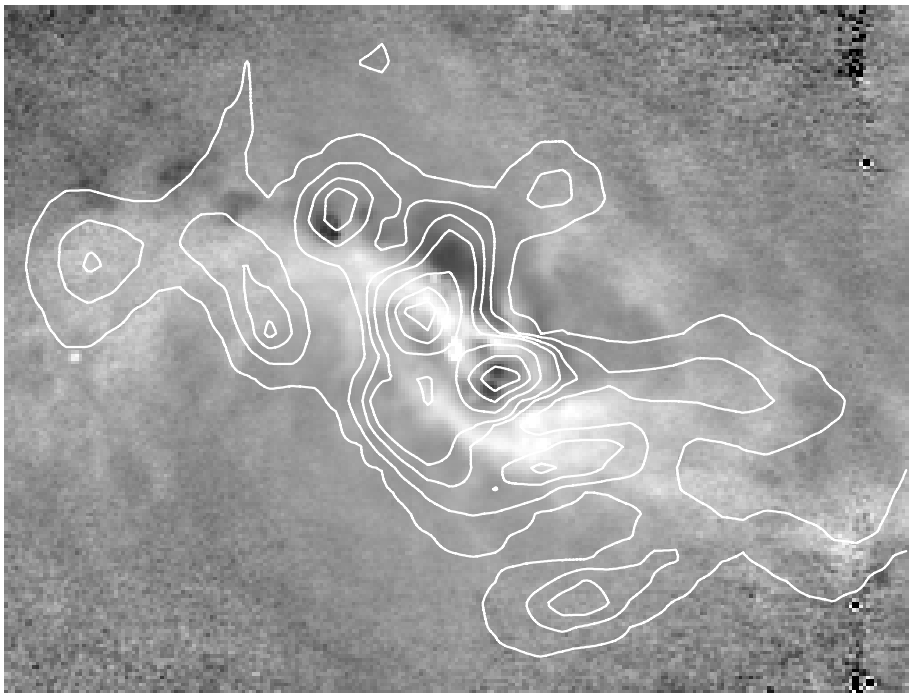

Fig. 6. *Contours:* SEST MEM map of NGC 1365 (effective resolution 5″) in the J = 3 – 2 CO line, centered on the optical nucleus and covering the bar (North is up and East to the left). The contour values are [0.01, 0.05, 0.1, 0.15, 0.3, 0.5, 0.7] × 958 K km s^{-1}. *Greyscale:* B – Gunn$z$ colour index image (124″ × 94″), which emphasizes the dust lanes (light areas) as well as hot-star- and H II-regions (dark areas)

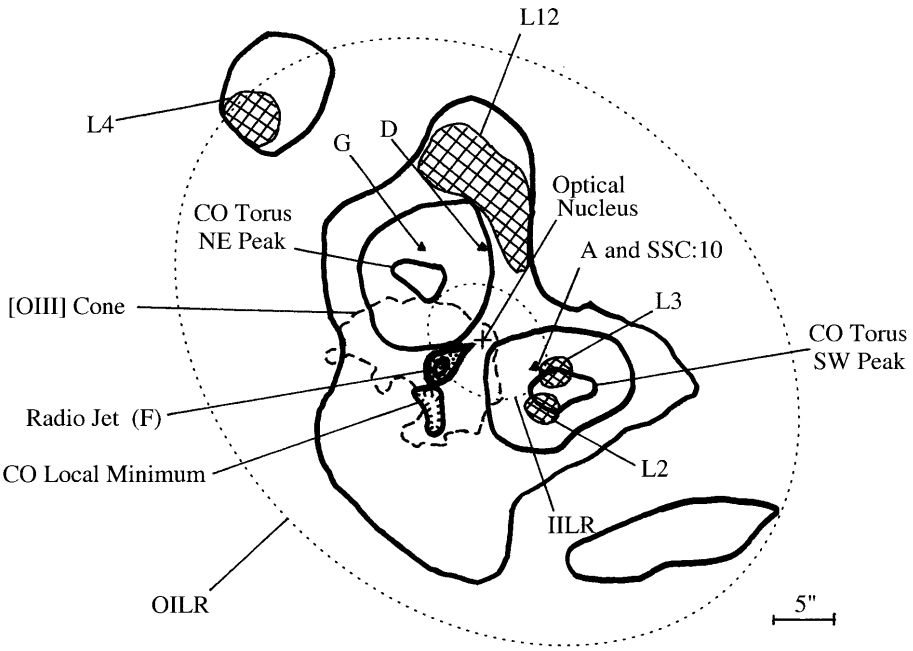

Fig. 7. Schematic diagram showing the different components in the nuclear region of NGC 1365. The optical nucleus – cross, CO distribution – solid contours, H II-regions and hot spots – hatched areas, radio supernovae and super star clusters – solid triangles, radio jet – wide solid contours, high-excitation [O III] cone – dashed contour, Outer Inner Lindblad Resonance (OILR) – large dotted ellipse, Inner Inner Lindblad Resonance (IILR) estimate – small dotted ellipse

The most interesting phenomenon, however, is the doubly-peaked CO structure seen near the optical nucleus, with a local minimum right at the nucleus. This structure and its alignment along the major axis of the galaxy is suggestive of a circumnuclear molecular torus with a radius of 5″ (450 pc). From the torus, there are CO extensions leading out into the two dominant eastern and western dust lanes.

The overall central CO velocity field was also presented by Sandqvist (1996). Here, we display only the position-velocity map along the major axis of the galaxy in Fig. 4. The velocity gradient across the molecular torus has its maximum value along the major axis and its character in this region may reflect rotation of the torus, which is in the same sense as that of the galaxy itself. A change of $J = 3 - 2$ CO peak-temperature velocity of 190 km s^{-1} is found over the 10″ between the two torus maxima. This velocity gradient is close to the corresponding optical velocity gradient of 205 km s^{-1} over the same 10″ (Sandqvist et al. 1995). It is almost twice that found in the earlier $J = 2-1$ CO observations, which, however, we simply attribute to the higher resolution of these $J = 3 - 2$ CO observations.

4. The Maximum Entropy Method (MEM) deconvolution

The angular resolution of the total integrated line intensity map has been improved by using a MEM deconvolution algorithm (Wilczek & Drapatz 1985). The SEST HPBW of the $J = 3 - 2$ CO observations was $15''$ and the observational grid spacing was generally $5''$ in the central region, i.e. appropriate for MEM-deconvolution. The best deconvolution was obtained after 14 smoothly converging iterations resulting in a χ^2-value of 5.7 for the final map. The expected resolution of the MEM map is about a third of the beamwidth used, i.e. $5''$.

The MEM map is presented in Fig. 5 and Fig. 6. In Fig. 5, the image has been rotated clockwise by 48°, so that the new x- and y-axes are the galaxy's minor and major axes, respectively. Here the deconvolved integrated intensities are displayed in a grey-scale representation to emphasize the detailed structure of the CO distribution. The major axis of the galaxy is the y-axis, which is the same as in Fig. 4, thus facilitating direct comparison of the molecular gas spatial and velocity structure along the major axis.

5. The molecular torus and other nuclear structure

A schematic overview of the different components in the nuclear region of NGC 1365 is presented in Fig. 7, which may facilitate the interpretation of the CO map from Figs. 5 and 6. The increased resolution of the CO MEM map strengthens the appearance of the circumnuclear molecular torus. The position of the coincident super star cluster SSC:10 and radio supernova A, mentioned in Sect. 1, lies very close to the southwestern molecular torus peak. This region thus contains three strong signatures of an intense starburst activity. Also the northeastern torus peak has suggested radio supernovae (D and G) in its immediate neighbourhood, although the identification with SSC:s is not as obvious due to the high optical extinction in this region.

Various CO extensions lead out from the torus into the two dominant eastern and western dust lanes of the bar, as well as into the H II-regions north and northeast of the nucleus. Distinct CO emission enhancement occurs near the positions of the two H II-regions L12 and L4 (Sandqvist et al. 1982), about $11''$ north and $23''$ northeast of the nucleus, respectively. Although it may be fortuitous, it is worthwhile pointing out that there is a secondary CO *minimum* near the positions of the radio jet and the conical shell of ionized [O III] gas, $5''$ southeast of the nucleus. Outside the ends of the jet and cone there is a secondary *maximum* of CO.

From hydrodynamical simulations of NGC 1365, Lindblad et al. (1996) have found that the radius of the Outer Inner Lindblad Resonance (OILR) in this galaxy is $27''$. The molecular torus peaks lie at an angular distance of only $6\farcs5$ (≈ 600 pc) from the nucleus, as measured on the MEM map, and the torus thus exists well inside the OILR, in fact in the vicinity of the expected Inner Inner Lindblad Resonance (IILR). Some velocity indications of orbit crowding of the molecular gas as it crosses the OILR have been presented by Sandqvist (1996).

In the past few years, interferometric CO observations have begun to yield a better understanding of the distribution of molecular gas in the nuclei of spiral galaxies. These results show that the molecular gas in the central regions of barred galaxies sometimes displays a "twin-peak" structure (e.g. Kenney 1996) located near the Inner Lindblad Resonances on the scale of 500–1000 pc. But also rings or partial rings, filled exponential disks, or small spirals are revealed in these regions for different galaxies. However, new surveys of normal galaxies indicate that bar-induced streaming is not the only mechanisms which can create a nuclear gas concentration (Sakamoto et al. 1998).

In a number of cases of barred spiral galaxies, the inward gas flow along the bar is predicted to be slowed down significantly near the Inner Lindblad Resonance resulting in a build-up of molecular gas concentrations in the region between the OILR and IILR (Combes 1988; Shlosman 1996). This effect seems to be present in NGC 1365, where the torus reaches its maximum concentration just outside the estimated IILR. However, in order to properly study the kinematic build-up of molecular gas concentrations between the OILR and IILR, we really need sensitive interferometric observations of the central region of this southern galaxy with such instruments as the proposed LSA/MMA.

Acknowledgements. I should like to thank Dr. L.-Å. Nyman at SEST for giving me extra observing time (during maintenance), so that the map could be finished in one observing session with exceptional submillimetre weather. I am also grateful for very useful discussions with Drs. P. Bergman and P.O. Lindblad.

References

Combes F., 1988, In: Pudritz R.E., Fich M. (eds.) Galactic and Extragalactic Star Formation. Kluwer, p. 475

Ghosh S.K., Verma R., Rengarajan T., Das B., Saraiya H., 1993, ApJS 86, 401

Hjelm M., Lindblad P.O., 1996, A&A 305, 727

Iyomoto N., Makishima K., Fukazawa Y., Tashiro M., Ishisahi Y., 1997, PASJ 49, 425

Jörsäter S., Lindblad P.O., 1989, In: Meurs E.J.A., Fosbury R.A.E. (eds.) ESO Conf. Workshop Proc. 32 Extranuclear Activity in Galaxies. p. 39

Jörsäter S., van Moorsel G., 1995, AJ 110, 2037

Jörsäter S., Lindblad P.O., Boksenberg A., 1984, A&A 140, 288

Kenney J., 1996, In: Buta R., Crocker D.A., Elmegreen B.G. (eds.) IAU Coll. 157, Barred Galaxies. ASP Conf. Ser. vol. 91, p. 150

Komossa S., Schulz H., 1998, A&A 339, 345

Kristen H., Jörsäter S., Lindblad P.O., Boksenberg A., 1997, A&A 328, 483

Kristen H., Sandqvist Aa., Lindblad P.O., 1998, In: Sofue Y. (ed.) IAU Symp. 184, The Central Region of the Galaxy and Galaxies. Kluwer, p. 277

Lindblad P.A.B., Lindblad P.O., Athanassoula E., 1996, A&A 313, 65

Lindblad P.O., 1999, A&AR (submitted)

Lonsdale C.J., Helou G., Good J.C., Rice W., 1985, Catalogued Galaxies and Quasars Observed in the IRAS Survey. Jet Propulsion Laboratory

Madore B.F., Freedman W.L., Silbermann N., et al., 1998, Nat 395:3, 47

Sakamoto K., Okumura S.K., Ishizuki S., Scoville N.Z., 1998, In: Sofue Y. (ed.) IAU Symp. 184, The Central Region of the Galaxy and Galaxies. Kluwer, p. 215
Sandqvist Aa., 1996, In: Sandqvist Aa., Lindblad P.O. (eds.) Barred Galaxies and Circumnuclear Activity – NOBEL SYMPOSIUM 98. Lecture Notes in Physics vol. 474, Springer, p. 133
Sandqvist Aa., Jörsäter S., Lindblad P.O., 1982, A&A 110, 336
Sandqvist Aa., Elfhag T., Jörsäter S., 1988, A&A 201, 223
Sandqvist Aa., Jörsäter S., Lindblad P.O., 1995, A&A 295, 585
Shlosman I., 1996, In: Sandqvist Aa., Lindblad P.O. (eds.) Barred Galaxies and Circumnuclear Activity – NOBEL SYMPOSIUM 98. Lecture Notes in Physics vol. 474, Springer, p. 141
Turner T.J., Urry C.M., Mushotzky R.F., 1993, ApJ 418, 653
Véron P., Lindblad P.O., Zuiderwijk E.J., Véron M.P., Adam G., 1980, A&A 87, 245
Wilczek R., Drapatz S., 1985, A&A 142, 9